Boundary spin polarization as robust signature of topological phase transition in Majorana nanowires

Marcel Serina, Daniel Loss, and Jelena Klinovaja

Department of Physics, University of Basel, Klingelbergstrasse 82, CH-4056 Basel, Switzerland

(Dated: March 2, 2018)

We show that the boundary charge and spin can be used as alternative signatures of the topological phase transition in topological models such as semiconducting nanowires with strong Rashba spin-orbit interaction in the presence of a magnetic field and in proximity to an *s*-wave superconductor. We identify signatures of the topological phase transition that do not rely on the presence of Majorana zero-energy modes and, thus, can serve as independent probes of topological properties. The boundary spin component along the magnetic field, obtained by summing contributions from all states below the Fermi level, has a pronounced peak at the topological phase transition point. Generally, such signatures can be observed at boundaries between topological and trivial sections in nanowires and are stable against disorder.

Introduction. Topological models have attracted a lot of attention in recent years. One of the first topological systems proposed about fourty years ago is the Su-Schrieffer-Heeger (SSH) model [1], describing properties of one-dimensional dimerized polymers. In this spinless model, a nondegenerate fermionic zero-mode, localized at a domain wall, is associated with a well-defined half-integer boundary charge [2, 3]. The same results can also be reproduced in a continuum model proposed by Jackiw and Rebbi [4]. The half-integer value of the boundary charge in these models is protected by the chiral symmetry. If this symmetry is broken, the value of the boundary charge can deviate from $e/2$ [5, 6]. Importantly, however, in the topological regime, there is always a boundary charge (independent of the presence of bound states) at the domain wall as was shown in several extensions of the SSH model [7–9]. Recently, the concept of the fractional boundary charge in topological SSH models was revisited, aiming at different systems that could be realized in modern experimental settings [10–28] and even in higher dimensions [29–31].

Currently, Majorana fermions (MFs), proposed as a real-field solution of the Dirac equation and thus being its own antiparticle [32], attract the most attention among the known bound states in topological systems. With the rapidly growing interest in topological properties of condensed matter systems [33–39], MFs were proposed to be present in various theoretical and experimental setups [40–56]. The most promising ones among them being chains of magnetic adatoms on superconducting surfaces [57–59] and semiconducting nanowires (NWs) with sizeable Rashba spin-orbit interaction (SOI) in the presence of a magnetic field and proximity-induced superconductivity [60–64]. Majorana fermions can be used as building blocks for topological quantum computing [65, 66] and can be combined with spin qubits in quantum dots into hybrid architectures [67–77].

Most of the studies [77–87] so far focused on the transport properties of such NWs in the topological regime or on properties of MFs themselves and their dependence
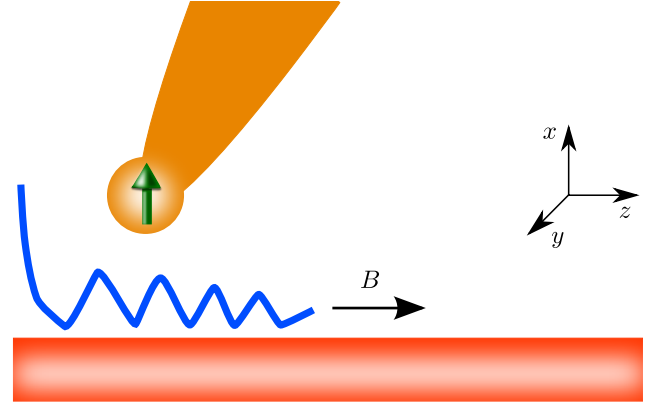

Figure 1. Our setup consists of a semiconducting NW (red bar) with Rashba SOI and with proximity-induced superconductivity due to coupling to a bulk *s*-wave superconductor (not shown). The SOI vector α points along the y direction. A magnetic field **B** applied along the NW axis is used to tune the system in and out of the topological phase. The boundary spin accumulates at the edges of the NW (blue curve) and can be used to identify the topological phase transition point. The magnetic signal can be measured by using *e.g.* NV centers (green arrow) on a tip (orange).

on physical parameters. Also, there has been substantial interest recently in the investigation of the spin polarization of Andreev and Majorana bound states [88, 89]. However, it has been pointed out that great care must be taken when identifying topological phases from the presence of quasiparticle states inside the superconducting gap [90–92]. Thus, it is most desirable to have additional signatures available (besides MFs) that would allow one to identify the topological phase transition. Motivated by this, we focus here on a different aspect of topological phases in one-dimensional systems, namely on non-transport signatures of the topological phase transition in the *bulk* states, or, more precisely, in the boundary charge and spin to which all occupied states close to the Fermi level contribute.

We will analyze the system depicted in Fig. 1 in tight-

binding description by means of exact diagonalization in which all four components of the quasiparticle wavefunctions are taken into account. Our findings are based on the properties of the bulk wavefunctions and are independent of the presence of MFs. In particular, we focus on the boundary spin in topological and trivial phases. Inspired by the approach in Ref. 93, we introduce the concept of boundary charge and spin and calculate these quantities for both phases. We find the signatures of critical behavior in components of the boundary spin, which allows us to identify the topological phase transition point.

Model. We investigate the system composed of a semi-conducting NW with strong Rashba SOI in the proximity to a bulk *s*-wave superconductor in the presence of a magnetic field B applied along the NW axis along z direction, see Fig. 1. The SOI vector α points along the y direction. The B-field results in the Zeeman energy $\Delta_Z = g\mu_B B/2$, where g is g-factor and μ_B the Bohr magneton. The corresponding tight-binding Hamiltonian is written as [82]

$$H = -t \sum_{\langle jj'\rangle\sigma} \left(c_{j\sigma}^\dagger c_{j'\sigma} + \text{H.c.}\right) + (2t-\mu)\sum_{j\sigma} c_{j\sigma}^\dagger c_{j\sigma}$$
$$+ \Delta_Z \sum_{j\sigma\sigma'} c_{j\sigma}^\dagger \sigma_z^{\sigma\sigma'} c_{j\sigma'} + i\sum_{\langle jj'\rangle\sigma\sigma'} \left(\alpha c_{j\sigma}^\dagger \sigma_y^{\sigma\sigma'} c_{j'\sigma'} + \text{H.c.}\right)$$
$$+ \Delta_{SC} \sum_j \left(c_{j\uparrow}^\dagger c_{j\downarrow}^\dagger + \text{H.c.}\right), \tag{1}$$

where the creation operator $c_{i\sigma}^\dagger$ creates an electron with spin $\sigma = \uparrow, \downarrow$ at site j of a chain consisting of N sites with lattice constant a. In the first and fourth terms, the summation runs only over neighbouring sites j and j'. Here, t denotes a nearest-neighbour hopping matrix element, μ is the chemical potential, and Δ_{SC} denotes the superconducting gap induced by proximity to the bulk *s*-wave superconductor. We note that in our model $\mu = 0$ corresponds the chemical potential being tuned to the SOI energy, which is defined here as $E_{SO} = \alpha^2/t$. For the rest of the paper we fix $t = 1$ and use it as an energy scale. The system is in the topological phase hosting zero-energy MFs at the nanowire ends if $\Delta_Z > \Delta_Z^c$, where $\Delta_Z^c = \sqrt{\mu^2 + \Delta_{SC}^2}$ [42, 43]. To study the topological phase transition in semiconducting NWs, we focus on the experimentally most relevant strong SOI regime, $E_{SO} \gg \Delta_{SC}, \Delta_Z$ [60, 64].

By diagonalizing numerically the Hamiltonian H [see Eq. (1)], one can determine the energy spectrum E_n. In addition, one also finds the operators $\psi_n = \sum_j \left(u_{\uparrow nj}^* c_{\uparrow j} + u_{\downarrow nj}^* c_{\downarrow j} + v_{\uparrow nj}^* c_{\uparrow j}^\dagger + v_{\downarrow nj}^* c_{\downarrow j}^\dagger\right)$, corresponding to annihilation operators for each of these $n = 4N$ states. Due to particle-hole symmetry, all states appear in pairs, *i.e.* if E_n is a solution, then so is $-E_n$. In what follows, we will focus on non-positive energy states. To characterize local bulk properties, we define the local charge ρ_j and the local spin densities $S_j^{x,y,z}$ at each site
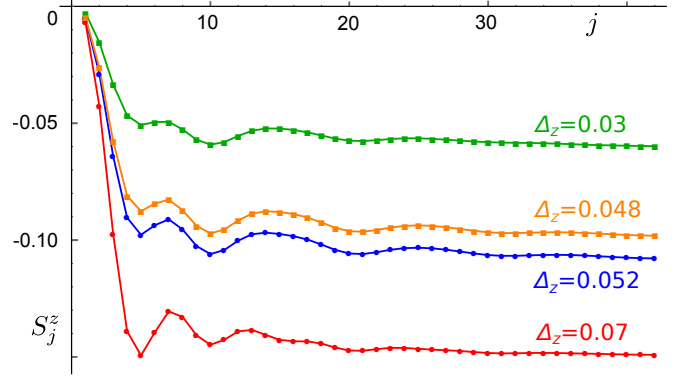

Figure 2. The spin density S_j^z (projecton along **B**-field) as a function of site j. Away from the NW ends, S_j^z is constant and given by S_0^z determined solely by bulk properties of the system. However, close to NW ends, S_j^z oscillates in all parameter regimes and there is no qualitative difference between trivial (indicated by dots) and topological (indicated by squares) phase. In all plots, the lines are guides to the eye. However, there is a quantitative shift in the amplitude of the first oscillations, as the system is driven through the topological phase transition. We consider the system being deep in (red, $\Delta_Z = 0.07$) and out of (green, $\Delta_Z = 0.03$) the topological phase as well as close to the topological phase transition in (blue, $\Delta_Z = 0.048$) and out of (orange, $\Delta_Z = 0.052$) the topological phase. The parameters are fixed to $N = 150$, $\mu = 0$, $\alpha = 0.3$, and $\Delta_{SC} = 0.05$.

as

$$\rho_j = \sum_{E_n<0;\sigma} \left(|u_{\sigma nj}|^2 - |v_{\sigma nj}|^2\right), \tag{2a}$$

$$S_j^z = \sum_{E_n<0;\sigma} \sigma\left(|u_{\sigma nj}|^2 - \sigma|v_{\sigma nj}|^2\right), \tag{2b}$$

$$S_j^x = \sum_{E_n<0;\sigma} \left(u_{\sigma nj}u_{\bar\sigma nj}^* - v_{\sigma nj}v_{\bar\sigma nj}^*\right), \tag{2c}$$

$$S_j^y = i\sum_{E_n<0;\sigma} \left(\sigma u_{\sigma nj}u_{\bar\sigma nj}^* - \sigma v_{\sigma nj}v_{\bar\sigma nj}^*\right), \tag{2d}$$

where the index $\sigma = 1$ ($\bar 1$) corresponds also to spin up (down) states defined above, see Fig. 2. For zero-energy MF wavefunctions one can show that $u_{\uparrow nj}^* = v_{\uparrow nj}$ and $u_{\downarrow nj}^* = v_{\downarrow nj}$. Thus, the MF charge and spin densities are exactly zero [94] and they do not contribute to Eq. (2). For this reason, we take in our definition only bulk states with negative energies into account. In addition, in our model, the Hamiltonian is real, so all the eigenvectors can also be chosen to be real. As a consequence, we find that S^y is identically zero for all configurations considered below.

Away for the NW ends, both spin and charge densities are constant as expected in a translationally invariant system, see Fig. 2. However, close to the NW end, these quantities oscillate around their bulk values ρ_0 and $S_0^{x,z}$ determined as the value at the middle of the NW $\rho_0 = \rho_{j=[\frac{N}{2}]}$ and $S_0^{x,z} = S_{j=[\frac{N}{2}]}^{x,z}$, where $[M]$ denotes

the integer part of M. Here, we assume that the NW is long enough such that these oscillations decay in the middle of the NW. In the strong SOI regime [87, 94], there are two lengthscales associated with bulk gaps at exterior branches $\xi_e/a = 2\alpha/\Delta_{SC}$ and interior branches $\xi_i/a = 2\alpha/|\Delta_{SC} - \Delta_Z|$. In what follows, we work in the regime in which the NW length L is much longer than both ξ_e and ξ_i, see Fig. 2.

Our main interest are boundary effects. As a result, for further convenience [93], we define the left and right boundary charge and spin as

$$\tilde{\rho}_{Lm} = \sum_{j=1}^{m} (\rho_j - \rho_0), \qquad (3)$$

$$\tilde{S}_{Lm}^{x,z} = \sum_{j=1}^{m} (S_j^{x,z} - S_0^{x,z}), \qquad (4)$$

$$\tilde{\rho}_{Rm} = \sum_{j=N-m}^{N} (\rho_j - \rho_0), \qquad (5)$$

$$\tilde{S}_{Rm}^{x,z} = \sum_{j=N-m}^{N} (S_j^{x,z} - S_0^{x,z}). \qquad (6)$$

First, we subtract from charge and spin densities their bulk values. Second, we sum densities over m sites at the left or right edge to define the right and left boundary charge or spin. Our system is symmetric with respect to the middle of the NW, so right and left boundary charges and spins can at most differ in sign. In our case, we find that $\tilde{\rho}_{Lm} = \tilde{\rho}_{Rm}$ and $\tilde{S}_{Lm}^z = \tilde{S}_{Rm}^z$, whereas $\tilde{S}_{Lm}^x = -\tilde{S}_{Rm}^x$, see the Supplemental Material for details [95]. We confirm that for values of m such that $\max\{\xi_e, \xi_i\}/a \ll m \ll N/2$, $\tilde{\rho}_m$ and $\tilde{S}_m^{x,z}$ converge to a constant values $\tilde{\rho}_{R,L}$ and $\tilde{S}_{R,L}^{x,z}$. Without loss of generality, in what follows, we focus only on the left boundary charge and spin.

Signature of topological phase transition. Next, we focus on the characteristic behavior of the boundary charge and spin around the topological phase transition. First, we analyze the behaviour of the spin density along the magnetic field S_j^z for various values of Zeeman gaps and all the other parameters fixed, see Fig. 2. As expected, S_j^z is constant in the middle of the chain and saturates to S_0^z, however, as one approaches the end of the chain, spatial oscillations in S_j^z begin to emerge. Not surprisingly, the spin polarization along the magnetic field strongly depends on the strength of the B-field. The stronger the magnetic field is, the larger is the polarization, see Fig. 2. Close to the phase transition point, the oscillations in S_j^z at the NW ends get more pronounced and are characterized by higher amplitudes and longer decay lengths. In order to quantify these oscillations, we calculate numerically the boundary spin and charge as defined in Eq. (4). The signature of the topological phase transition can be clearly seen in the z-component of the
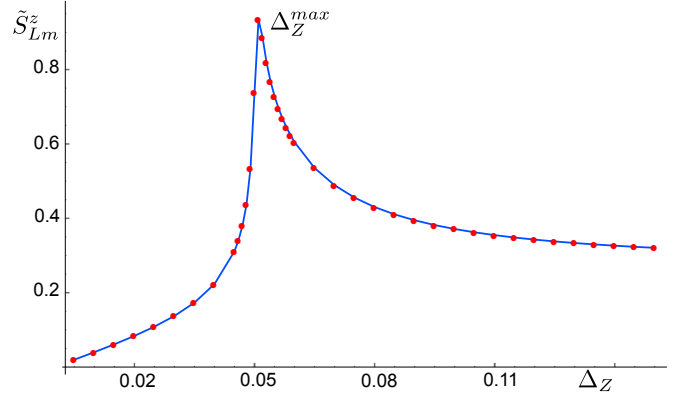

Figure 3. The left boundary spin component along z direction, $\tilde{S}_{Lm}^z$, [see Eq. (4)] as a function of the Zeeman energy Δ_Z. The $\tilde{S}_{Lm}^z$ has a peak at Δ_Z^{max}, which coincides in sufficiently long systems with the point of the topological phase transition $\Delta_Z = \Delta_{SC}$. This peak is an independent signature of the topological phase transition. The system parameters are taken to be $\alpha = 0.3, \Delta_{SC} = 0.05, \mu = 0, N = 2000,$ and $m = 1000$.

boundary spin, $S_{L/Rm}^z$, see Fig. 3. In the SM [95], we also provide details on the boundary charge and the S^x-component, however, there is no signature of the topological phase transition in these quantities. In contrast to that, the $S_{L/Rm}^z$ has a pronounced peak at the value of the Zeeman energy Δ_Z^{max} that is very close to the critical value Δ_Z^c determined from the topological criterion. The longer the system is, the more close Δ_Z^{max} to Δ_Z^c, see Fig. 4. We find that Δ_Z^{max} weakly depends on the system size N and approaches the critical value asymptotically as a function of $1/N$. Importantly, the value of $S_{L/Rm}^z$ does not depend on whether the MF state is occupied or
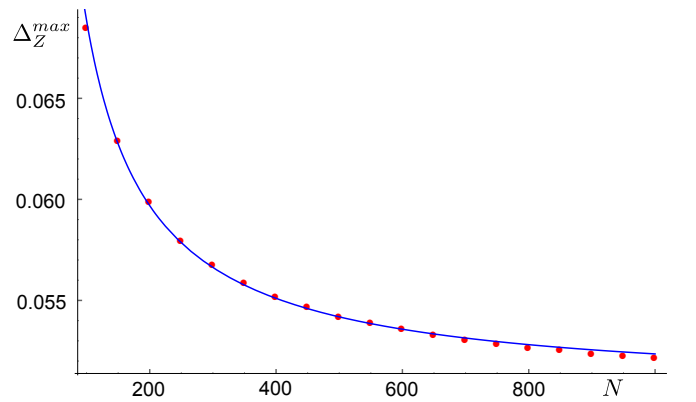

Figure 4. The position of the peak Δ_Z^{max} in $\tilde{S}_{Lm}^z$ [see Eq. (4)] as a function of system size N. As the system size is increases, Δ_Z^{max} gets more and more close to the critical value Δ_Z^c at which the topological phase transition takes place. We find that the obtained numerically results (red dots) can be fitted the best with the analytical formula $(\Delta_Z^{max} - \Delta_Z^c) \propto 1/N$ (blue curve). The system parameters are the same as in Fig. 3 with $m = N/2$.
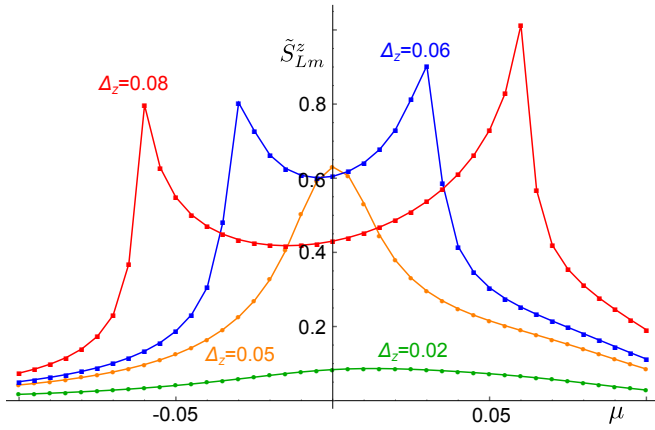
Figure 5. The z component of the boundary spin $\tilde{S}^z_{Lm}$ [see Eq. (4)] as a function of the chemical potential μ. In the topological regime, there are two peaks corresponding to two critical values of the chemical potential $\pm\mu_c$, at which the system goes through the topological phase transition. In the trivial regime such peaks are absent as the system cannot be tuned into the topological phase. Far from the transition point (green, $\Delta_Z = 0.02$) there is a broad maximum in $\tilde{S}^z_{Lm}$ which gets more pronounced as system approaches the topological phase transition (orange, $\Delta_Z = 0.05$) and develops later into a double peak structure (blue, $\Delta_Z = 0.06$ and red, $\Delta_Z = 0.08$) in the topological phase. The system parameters are fixed to $N = 1000$, $\alpha = 0.3$, $\Delta_{SC} = 0.05$, and $m = 500$.

not as its contribution is identically zero. Thus, for long enough systems, the position of the peak in $S^z_{L/Rm}$ can be used as an independent signature of the topological phase transition.

It is also important to emphasize the role of the chemical potential μ. It is well known that the system can also be driven between topological and trivial phases by changing μ [42, 43]. In this case, when the topological phase is reached, there are two peaks in $\tilde{S}^z_{Lm}$ at two critical values $\mu = \pm\mu^c$ with $\mu_c = \sqrt{\Delta_Z^2 - \Delta_{SC}^2}$, see Fig. 5. Again, we see that the critical values $\pm\mu_c$ are asymptotically reached as the size of the system is increased. However, when the width of two peaks is comparable with μ_c, the two peaks will merge. Thus, this criterion works best for large values of Δ_Z and long systems. We note that one faces the same problem if the detection of the phase transition is done via zero-bias peak signatures in transport measurments. In short nanowires, the MFs of opposite ends will overlap and split away from zero energy if one is not deeply in the topological phase.

Finally, we would like to demonstrate the stability of the presented signatures against disorder and, thus, show that they are also topologically protected. For this, we add on-site disorder to our model [see Eq. (1)] as well as we modify the system by adding trivial section at the NW end. Results for the both cases are presented in the SM [95]. In all configurations, the signature of the topological phase transition in the boundary spin $\tilde{S}^z_{Lm}$ is

still fully present.

So far we have focused on signatures of the topological phase transition to be detected in the boundary spin. However, the bulk values of the spin component along the magnetic field S^z_0 also carry information about the topological phase transition if periodic boundary conditions are imposed, see the SM for details [95]. In this case, the system is translationally invariant and it does not matter at which point one computes the bulk value of the spin component S^z_{PBC}. The signature of the topological phase transition is still present but different. In particular, there is now a sharp discontinuity in S^z_{PBC} with a jump of order $1/N$ at the point of the topological phase transition, $\Delta_Z = \Delta_Z^c$, see the SM [95].

The measurement of boundary spins will be challenging but seems to be within reach for state-of-the-art magnetometry with NV-centers, spin-polarized STM tips, or nanoSQUIDs [96–102]. We furthermore recall that it is the total integral over the spin density within the localization length that determines the spin signature of the phase transition. Thus, a resolution of the measurement device over this length scale should be sufficient.

Conclusions. We have identified signatures of the topological phase transition in the boundary spin component in one-dimensional topological systems. These signatures are present when tuning through the phase transition point either with the magnetic field or with the chemical potential. Moreover, we have shown that these signatures do not rely on the presence of MFs and always occur at the boundary between topological and trivial sections of the NW. We have analyzed the finite-size effects of the boundary spin and shown that the position of the peak converges to the value obtained analytically in the continuum limit. These results are also stable with respect to disorder.

[1] W. P. Su, J. R. Schrieffer, and A. J. Heeger, Phys. Rev. Lett. **42**, 1698 (1979).
[2] W. P. Su and J. R. Schrieffer, Phys. Rev. Lett. **46**, 738 (1981).
[3] J. Goldstone and F. Wilczek, Phys. Rev. Lett. **47**, 986 (1981).
[4] R. Jackiw and C. Rebbi, Phys. Rev. D **13**, 3398 (1976).
[5] R. Jackiw and J. Schrieffer, Nuclear Physics B **190**, 253 (1981).
[6] W. P. Su and J. R. Schrieffer, Phys. Rev. Lett. **46**, 738 (1981).

[7] M. J. Rice and E. J. Mele, Phys. Rev. Lett. **49**, 1455 (1982).

[8] R. Jackiw and G. Semenoff, Phys. Rev. Lett. **50**, 439 (1983).

[9] S. Kivelson, Phys. Rev. B **28**, 2653 (1983).

[10] X.-L. Qi, T. L. Hughes, and S.-C. Zhang, Nature Physics **4**, 273 (2008).

[11] N. Goldman, I. Satija, P. Nikolic, A. Bermudez, M. A. Martin-Delgado, M. Lewenstein, and I. B. Spielman, Phys. Rev. Lett. **105**, 255302 (2010).

[12] S. Gangadharaiah, L. Trifunovic, and D. Loss, Phys. Rev. Lett. **108**, 136803 (2012).

[13] Y. E. Kraus, Y. Lahini, Z. Ringel, M. Verbin, and O. Zilberberg, Phys. Rev. Lett. **109**, 106402 (2012).

[14] J. Klinovaja, P. Stano, and D. Loss, Phys. Rev. Lett. **109**, 236801 (2012).

[15] J. C. Budich and E. Ardonne, Phys. Rev. B **88**, 035139 (2013).

[16] Z. Xu, L. Li, and S. Chen, Phys. Rev. Lett. **110**, 215301 (2013).

[17] F. Grusdt, M. Höning, and M. Fleischhauer, Phys. Rev. Lett. **110**, 260405 (2013).

[18] J. Klinovaja and D. Loss, Phys. Rev. Lett. **110**, 126402 (2013).

[19] K. A. Madsen, E. J. Bergholtz, and P. W. Brouwer, Phys. Rev. B **88**, 125118 (2013).

[20] A. V. Poshakinskiy, A. N. Poddubny, L. Pilozzi, and E. L. Ivchenko, Phys. Rev. Lett. **112**, 107403 (2014).

[21] D. Rainis, A. Saha, J. Klinovaja, L. Trifunovic, and D. Loss, Phys. Rev. Lett. **112**, 196803 (2014).

[22] J. Klinovaja and D. Loss, Phys. Rev. Lett. **112**, 246403 (2014).

[23] R. Wakatsuki, M. Ezawa, Y. Tanaka, and N. Nagaosa, Phys. Rev. B **90**, 014505 (2014).

[24] P. Marra, R. Citro, and C. Ortix, Phys. Rev. B **91**, 125411 (2015).

[25] J. Klinovaja and D. Loss, The European Physical Journal B **88**, 62 (2015).

[26] G. van Miert and C. Ortix, Phys. Rev. B **96**, 235130 (2017).

[27] B. Pérez-González, M. Bello, A. Gómez-León, and G. Platero, arXiv:1802.03973.

[28] S. Ryu, C. Mudry, C. Hou, and C. Chamon, Phys. Rev. B **80**, 205319 (2009).

[29] B. Seradjeh, C. Weeks, and M. Franz, Phys. Rev. B **77**, 033104 (2008).

[30] A. Rüegg and G. A. Fiete, Phys. Rev. B **83**, 165118 (2011).

[31] P. Szumniak, J. Klinovaja, and D. Loss, Phys. Rev. B **93**, 245308 (2016).

[32] E. Majorana, Nuovo Cimento **14**, 171 (1937).

[33] B. A. Volkov and O. Pankratov, Pi'sma Zh. Eksp. Teor. Fiz. **42**, 145 (1985).

[34] B. A. Bernevig, T. L. Hughes, and S.-C. Zhang, Science **314**, 1757 (2006).

[35] M. König, S. Wiedmann, C. Brüne, A. Roth, H. Buhmann, L. W. Molenkamp, X.-L. Qi, and S.-C. Zhang, Science **318**, 766 (2007).

[36] L. Fu, C. L. Kane, and E. J. Mele, Phys. Rev. Lett. **98**, 106803 (2007).

[37] A. Roth, C. Brüne, H. Buhmann, L. W. Molenkamp, J. Maciejko, X.-L. Qi, and S.-C. Zhang, Science **325**, 294 (2009).

[38] M. Z. Hasan and C. L. Kane, Rev. Mod. Phys. **82**, 3045

[39] T. A. Bernevig and T. L. Hughes, *Topological Insulators and Topological Superconductors* (Princeton University Press, 2013).

[40] L. Fu and C. L. Kane, Phys. Rev. Lett. **100**, 096407 (2008).

[41] M. Sato and S. Fujimoto, Phys. Rev. B **79**, 094504 (2009).

[42] R. M. Lutchyn, J. D. Sau, and S. Das Sarma, Phys. Rev. Lett. **105**, 077001 (2010).

[43] Y. Oreg, G. Refael, and F. von Oppen, Phys. Rev. Lett. **105**, 177002 (2010).

[44] J. Alicea, Phys. Rev. B **81**, 125318 (2010).

[45] A. C. Potter and P. A. Lee, Phys. Rev. B **83**, 094525 (2011).

[46] J. Klinovaja, S. Gangadharaiah, and D. Loss, Phys. Rev. Lett. **108**, 196804 (2012).

[47] D. Chevallier, D. Sticlet, P. Simon, and C. Bena, Phys. Rev. B **85**, 235307 (2012).

[48] S. Nadj-Perge, I. K. Drozdov, B. A. Bernevig, and A. Yazdani, Phys. Rev. B **88**, 020407 (2013).

[49] F. Pientka, L. I. Glazman, and F. von Oppen, Phys. Rev. B **88**, 155420 (2013).

[50] J. Klinovaja, P. Stano, A. Yazdani, and D. Loss, Phys. Rev. Lett. **111**, 186805 (2013).

[51] B. Braunecker and P. Simon, Phys. Rev. Lett. **111**, 147202 (2013).

[52] M. M. Vazifeh and M. Franz, Phys. Rev. Lett. **111**, 206802 (2013).

[53] M. Thakurathi, A. A. Patel, D. Sen, and A. Dutta, Phys. Rev. B **88**, 155133 (2013).

[54] F. Maier, J. Klinovaja, and D. Loss, Phys. Rev. B **90**, 195421 (2014).

[55] F. Setiawan, K. Sengupta, I. B. Spielman, and J. D. Sau, Phys. Rev. Lett. **115**, 190401 (2015).

[56] G. L. Fatin, A. Matos-Abiague, B. Scharf, and I. Žutić, Phys. Rev. Lett. **117**, 077002 (2016).

[57] S. Nadj-Perge, I. K. Drozdov, J. Li, H. Chen, S. Jeon, J. Seo, A. H. MacDonald, B. A. Bernevig, and A. Yazdani, Science **346**, 602 (2014).

[58] M. Ruby, F. Pientka, Y. Peng, F. von Oppen, B. W. Heinrich, and K. J. Franke, Phys. Rev. Lett. **115**, 197204 (2015).

[59] R. Pawlak, M. Kisiel, J. Klinovaja, T. Meier, S. Kawai, T. Glatzel, D. Loss, and E. Meyer, Npj Quantum Information **2**, 16035 (2016).

[60] V. Mourik, K. Zuo, S. M. Frolov, S. R. Plissard, E. P. A. M. Bakkers, and L. P. Kouwenhoven, Science **336**, 1003 (2012).

[61] A. Das, Y. Ronen, Y. Most, Y. Oreg, M. Heiblum, and H. Shtrikman, Nature Physics **8**, 887 (2012).

[62] L. P. Rokhinson, X. Liu, and J. K. Furdyna, Nature Physics **8**, 795 (2012).

[63] H. O. H. Churchill, V. Fatemi, K. Grove-Rasmussen, M. T. Deng, P. Caroff, H. Q. Xu, and C. M. Marcus, Phys. Rev. B **87**, 241401 (2013).

[64] S. M. Albrecht, A. P. Higginbotham, M. Madsen, F. Kuemmeth, T. S. Jespersen, J. Nygård, P. Krogstrup, and C. M. Marcus, Nature **531**, 206 (2016).

[65] A. Y. Kitaev, Annals of Physics **303**, 2 (2003).

[66] C. Nayak, S. H. Simon, A. Stern, M. Freedman, and S. Das Sarma, Rev. Mod. Phys. **80**, 1083 (2008).

[67] K. Flensberg, Phys. Rev. Lett. **106**, 090503 (2011).

[68] D. E. Liu and H. U. Baranger, Phys. Rev. B **84**, 201308

(2010).

(2011).

[69] E. Vernek, P. H. Penteado, A. C. Seridonio, and J. C. Egues, Phys. Rev. B **89**, 165314 (2014).

[70] S. Hoffman, C. Schrade, J. Klinovaja, and D. Loss, Phys. Rev. B **94**, 045316 (2016).

[71] M. T. Deng, S. Vaitiekenas, E. B. Hansen, J. Danon, M. Leijnse, K. Flensberg, J. Nygård, P. Krogstrup, and C. M. Marcus, Science **354**, 1557 (2016).

[72] L. S. Ricco, Y. Marques, F. A. Dessotti, R. S. Machado, M. de Souza, and A. C. Seridonio, Phys. Rev. B **93**, 165116 (2016).

[73] F. A. Dessotti, L. S. Ricco, Y. Marques, L. H. Guessi, M. Yoshida, M. S. Figueira, M. de Souza, P. Sodano, and A. C. Seridonio, Phys. Rev. B **94**, 125426 (2016).

[74] L. A. Landau, S. Plugge, E. Sela, A. Altland, S. M. Albrecht, and R. Egger, Phys. Rev. Lett. **116**, 050501 (2016).

[75] C. Schrade, S. Hoffman, and D. Loss, Phys. Rev. B **95**, 195421 (2017).

[76] L. Xu, X.-Q. Li, and Q.-F. Sun, Journal of Physics: Condensed Matter **29**, 195301 (2017).

[77] E. Prada, R. Aguado, and P. San-Jose, Phys. Rev. B **96**, 085418 (2017).

[78] L. Fu and C. L. Kane, Phys. Rev. Lett. **102**, 216403 (2009).

[79] E. Prada, P. San-Jose, and R. Aguado, Phys. Rev. B **86**, 180503 (2012).

[80] J. S. Lim, R. López, and L. Serra, New Journal of Physics **14**, 083020 (2012).

[81] A. A. Zyuzin, D. Rainis, J. Klinovaja, and D. Loss, Phys. Rev. Lett. **111**, 056802 (2013).

[82] D. Rainis, L. Trifunovic, J. Klinovaja, and D. Loss, Phys. Rev. B **87**, 024515 (2013).

[83] A. Zazunov, A. Altland, and R. Egger, New Journal of Physics **16**, 015010 (2014).

[84] L. Weithofer, P. Recher, and T. L. Schmidt, Phys. Rev. B **90**, 205416 (2014).

[85] F. m. c. Crépin, B. Trauzettel, and F. Dolcini, Phys. Rev. B **89**, 205115 (2014).

[86] W. S. Cole, J. D. Sau, and S. Das Sarma, Phys. Rev. B **94**, 140505 (2016).

[87] P. Szumniak, D. Chevallier, D. Loss, and J. Klinovaja, Phys. Rev. B **96**, 041401 (2017).

[88] D. Sticlet, C. Bena, and P. Simon, Phys. Rev. Lett. **108**, 096802 (2012).

[89] M. Guigou, N. Sedlmayr, J. M. Aguiar-Hualde, and C. Bena, EPL **115**, 47005 (2016).

[90] D. Stanescu and S. Tewari, Journal of the Indian Institute of Science **96**, 107 (2016).

[91] C.-X. Liu, J. D. Sau, T. D. Stanescu, and S. Das Sarma, Phys. Rev. B **96**, 075161 (2017).

[92] C. Moore, T. D. Stanescu, and S. Tewari, arXiv:1711.06256.

[93] J.-H. Park, G. Yang, J. Klinovaja, P. Stano, and D. Loss, Phys. Rev. B **94**, 075416 (2016).

[94] J. Klinovaja and D. Loss, Phys. Rev. B **86**, 085408 (2012).

[95] See the Supplemental material.

[96] W. Wernsdorfer, Superconductor Science and Technology **22**, 064013 (2009).

[97] P. Stano, J. Klinovaja, A. Yacoby, and D. Loss, Phys. Rev. B **88**, 045441 (2013).

[98] T. Staudacher, F. Shi, S. Pezzagna, J. Meijer, J. Du, C. A. Meriles, F. Reinhard, and J. Wrachtrup, Science **339**, 561 (2013).

[99] L. Trifunovic, F. L. Pedrocchi, S. Hoffman, P. Maletinsky, A. Yacoby, and D. Loss, Nature Nanotechnology **10**, 541 (2015).

[100] M. J. Martínez-Pérez, B. Müller, D. Schwebius, D. Korinski, R. Kleiner, J. Sesé, and D. Koelle, Superconductor Science and Technology **30**, 024003 (2017).

[101] L. Thiel, D. Rohner, M. Ganzhorn, P. Appel, E. Neu, B. Müller, R. Kleiner, D. Koelle, and P. Maletinsky, Nature Nanotechnology **11**, 677 (2016).

[102] S. Jeon, Y. Xie, J. Li, Z. Wang, B. Bernevig, and A. Yazdani, Science **358**, 772 (2017).

Supplemental Material to 'Boundary spin polarization as robust signature of topological phase transition in Majorana nanowires'

Marcel Serina, Daniel Loss, and Jelena Klinovaja

Department of Physics, University of Basel, Klingelbergstrasse 82, CH-4056 Basel, Switzerland

Results for boundary spin component S_{Lm}^x and boundary charge ρ_{Lm}

For the sake of completeness, we present here our results for the local spin density S_j^x and charge density ρ_j, see Fig. 6. As the SOI vector points along the x direction, it is expected that S_j^x in the center of the chain vanishes and moreover $\sum_{j=1}^{N} S_j^x = 0$, which imposes that S_j^x must be antisymmetric with respect to the middle of the chain. We confirm this expectation by exact numerical diagonlization. As in the case of S_j^z, spatial oscillations in S_j^x appear close to the ends of the NW, getting more pronounced as one approaches the topological phase transition. In case of the charge density ρ_j, the characteristic behavior is very similar while in this case, as expected, the results are symmetric with respect to the middle of the wire. We also calculate the corresponding boundary charge $\tilde{\rho}_{Lm}$ and the boundary spin component $\tilde{S}_{Lm}^x$ (see Fig. 7). However, we do not observe any well-pronounced signatures of the topological phase transition in these quantities. For $\tilde{\rho}_{Lm}$, we can see a transition from almost constant to a linear dependence of Δ_Z, however, this signature seems to be difficult to measure.
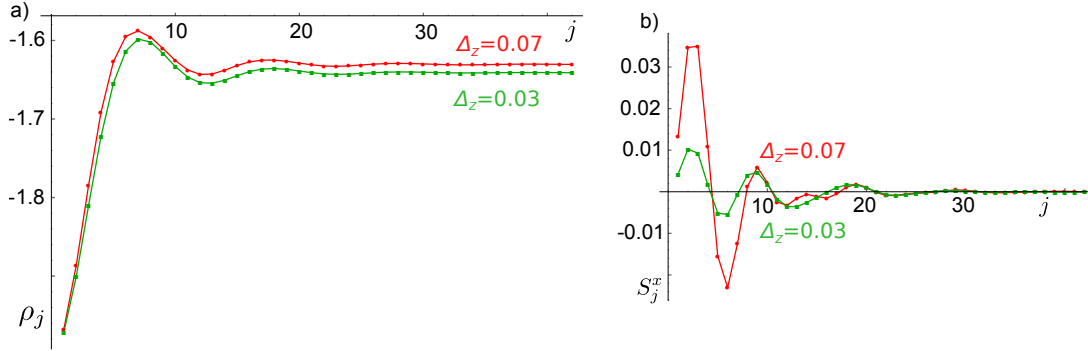

Figure 6. (a) Charge density ρ_j and (b) component of the spin density along the x axis, S_j^x, as a function of site position j. The characteristic features are similar to those of S_j^z discussed in the main text, again there are oscillations close to the NW ends in both trivial and topological phases. However, neither the amplitude of the first oscillation does not differ between the two phases [see (a)] nor the oscillations tend to cancel each other [see (b)]. Results for the trivial (topological) phase are marked by green squares (red cycles) and correspond to $\Delta_Z = 0.03$ ($\Delta_Z = 0.07$). The system parameters are chosen to be $N = 150$, $\mu = 0$, $\alpha = 0.3$, $\Delta_{SC} = 0.05$.
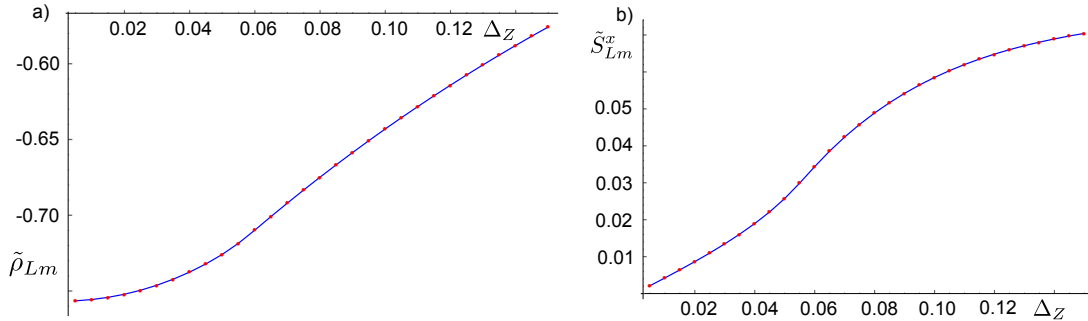

Figure 7. (a) Boundary charge $\tilde{\rho}_{Lm}$ and (b) component of the boundary spin along the x axis $\tilde{S}_{Lm}^x$ as a function of Zeeman energy Δ_Z. There are only weak features associated with the topological phase transition. Unlike the pronounced peak in $\tilde{S}_{Lm}^z$, the component $\tilde{S}_{Lm}^x$ cannot reliably distinguish the trivial from topological phase. The system parameters are chosen to be $\alpha = 0.3$, $\Delta_{SC} = 0.05$, $\mu = 0$, $N = 200$, and $m = 100$.
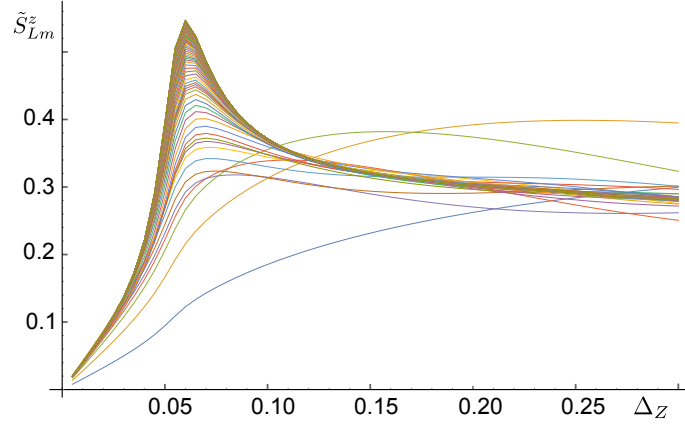
Figure 8. Component of the boundary spin along z axis, $\tilde{S}^z_{Lm}$, [see Eq. (4)] as a function of Zeeman energy Δ_Z for different cut-off values: $m = 1, ..., 100$. Here, $m = 1$ corresponds to the lowest blue curve. Other curves are ordered according to ascending m at small Δ_Z. The peak in $\tilde{S}^z_{Lm}$ close to Δ^c_Z is observed already for $m = \xi_{SC}/a$ ($\xi_{SC}/a = 12$ for this plot), thus, the proposed signature of the topological phase transition is local with contributions coming from the occupied bulk states at the end of the NW. The system parameters are chosen to be $N = 200$, $\alpha = 0.3$, $\Delta_{SC} = 0.05$, and $\mu = 0$.

Local properties of boundary spin component $\tilde{S}^z_{Lm}$

We would like to elaborate on the question in which sense $\tilde{S}^z_{Lm}$ is a *local* signature emerging only at the end of the NW. In other words, we should investigate the behavior of $\tilde{S}^z_{Lm}$ with respect to changes in m, see Fig. 8. Far from the topological phase transition, we observe that $\tilde{S}^z_{Lm}$ converges very quickly with increasing m and is therefore a local property of the end of the NW. As we approach the transition point, values for the respective m's start to differ. Nevertheless, even for $m = 20$ we still observe a well-pronounced peak almost at the same Δ_Z as for $m = 100$. Based on that we can conclude that $\tilde{S}^z_{Lm}$ is a local quantity with main support at the end of the NW.

Effect of on-site disorder - stability of topological phase transition signature in $\tilde{S}^z_{Lm}$

To demonstrate that the presented signature of the topological phase transition in the boundary spin component $\tilde{S}^z_{Lm}$ is robust, we must verify that this signature persists even if the disorder is present, see Fig. 9. We perform the same calculations as before, however, add fluctuations in the chemical potential. We see that, locally, disorder
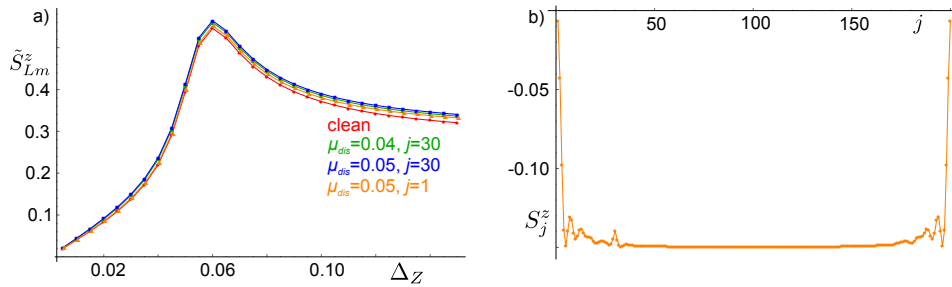

Figure 9. (a) Component of the boundary spin, $\tilde{S}^z_{Lm}$, and (b) the z-component of the local spin density S^z_j in the system with on-site disorder. Generally, we observe the same behavior as in the clean case, accompanied by small overall renormalization of $\tilde{S}^z_{Lm}$ even in the case of relatively strong disorder. We add disorder in the chemical potential μ_{dis} on site j, elsewhere, we keep $\mu = 0$. In panel (a), $\tilde{S}^z_{Lm}$ for the clean wire (red) is compared with results for a disordered wire with $\mu_{dis} = 0.04$ at site $j = 30$ (green); with $\mu_{dis} = 0.05$ at site $j = 30$ (blue); and with $\mu_{dis} = 0.04$ at site $j = 1$ (orange). The signature of the topological phase transition is clearly not affected by disorder. In panel (b), S^z_j is shown for a disordered NW with $\mu_{dis} = 0.04$ at site $j = 30$ ($\Delta_Z = 0.07$). The presence of the impurity manifests itself as an additional local peak in S^z_j accompanied by spatial oscillations. As a result, there is a local redistribution of the spin density, which does not affect the boundary spin. If there are several impurities, their contributions average out and the system gets even more stable to disorder. The system parameters are chosen to be $N = 200$, $\alpha = 0.3$, $\Delta_{SC} = 0.05$, and $m = 100$.
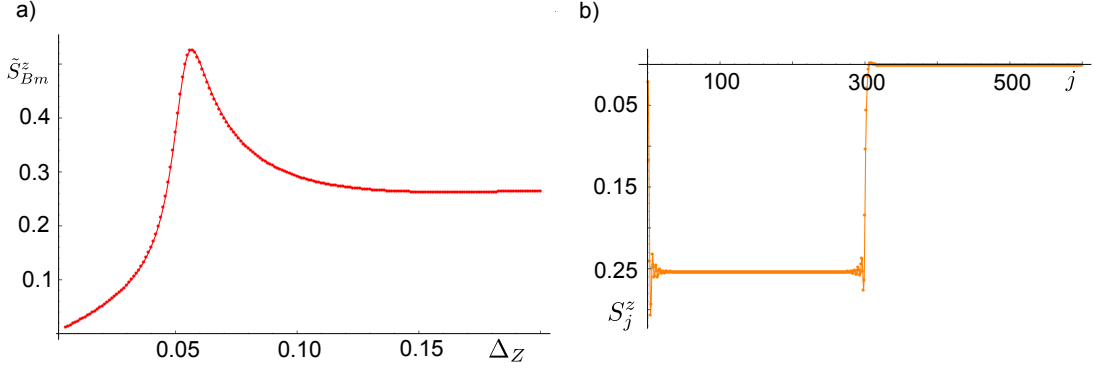
Figure 10. (a) Component of the boundary spin, $\tilde{S}^z_{Bm}$, and (b) the z-component of the local spin density S^z_j. The right section of the NW corresponds to a superconducting lead, in which we fix $\alpha = \Delta_Z = 0$. In contrast to that, the left section of the NW is described by $\alpha = 0.3$. The chemical potential is uniform, $\mu = 0$, as well as the superconducting strength $\Delta_{SC} = 0.05$. In addition, $N_< = N_> = 300$ and $m_< = m_> = 150$. (a) Again, there is a signature of the topological phase transition in $\tilde{S}^z_{Bm}$. (b) The boundary spin has contributions from both topological and trivial sections of the NW ($\Delta_Z = 0.15$). We also note that the bulk values of spin density S^z_j are different in two sections.

causes the appearance of a similar feature in the spin density as already observed at the NW ends. Namely, there is a local maximum in the spin density S^z_j at the position of the impurity. The oscillations around the impurity position decay as one moves away. If there are many impurities, such effects will average out. As a result, there can be only local redistribution of the spin density S^z_j, which do not affect the boundary spin $\tilde{S}^z_{Lm}$. Therefore, as expected, the signature of the topological phase transition, *i.e.* peak in $\tilde{S}^z_{Lm}$ at Δ^c_Z, is robust against local disorder. This holds also in the case of disorder as strong as the superconducting gap Δ_{SC} itself and well beyond.

Boundary spin $\tilde{S}^z_{Rm}$ at the boundary between topological and trivial phases

In the main text, we have focused on the boundary spin located at the ends of the NW. Here, we show that, generally, the boundary spin is associated with the boundary between topological and trivial sections in the NW. As a result, there is a contribution to $\tilde{S}^z_{L/Rm}$ coming from both sides of the boundary, *i.e.* from the topological section and from the trivial section. This means that the definitions for $\tilde{S}^z_{R/Lm}$ given by Eqs. (4) and (6) should be generalized. For the moment, let us focus on the boundary located at the site N and introduce the boundary spin as

$$\tilde{S}^z_{Bm} = \sum_{j=N-m_<}^{N} \left(S^z_j - S^z_{0<}\right) - \sum_{j=N+1}^{N+m_>} \left(S^z_j - S^z_{0>}\right), \quad S^z_{0<} = S^z_{j=[\frac{N_\le}{2}]}, \quad S^z_{0>} = S^z_{j=[N_< + \frac{N_\ge}{2}]}. \tag{7}$$

Here, the sum runs over $m_<$ ($m_>$) sites of the left (right) section of the NW consisting in total of $N_<$ ($N_>$) sites, such that $m = m_< + m_>$. Without loss of generality, we can assume that the left (right) section is in the topological (trivial) phase. Assuming that both sections are long enough, one determines the bulk value of the spin density as $S^z_{0<}$ and $S^z_{0>}$ for each section separately, as they are generally not the same. This can be seen clearly in Figs. 11(b) and 10(b), where we show how a typical spin density profile looks like in NWs divided into two sections.

We consider two scenarios. In the first scenario (see Fig. 10), we attach a superconducting lead at the right end of the NW. In this lead, we assume that the Zeeman field is screened and the SOI is absent. As a result, this NW section is always in the trivial phase. Again, one observes a well-pronounced peak in $\tilde{S}^z_{Bm}$ at Zeeman energies close to the critical value Δ^c_Z. In the second scenario (see Fig. 11), the right section of the NW has stronger proximity-induced superconductivity. Thus, it enters the topological phase at larger values of Zeeman energy. As a result, there are two peaks in $\tilde{S}^z_{Bm}$. The first (second) peak corresponds to a Zeeman energy at which left (right) section of the NW becomes topological.
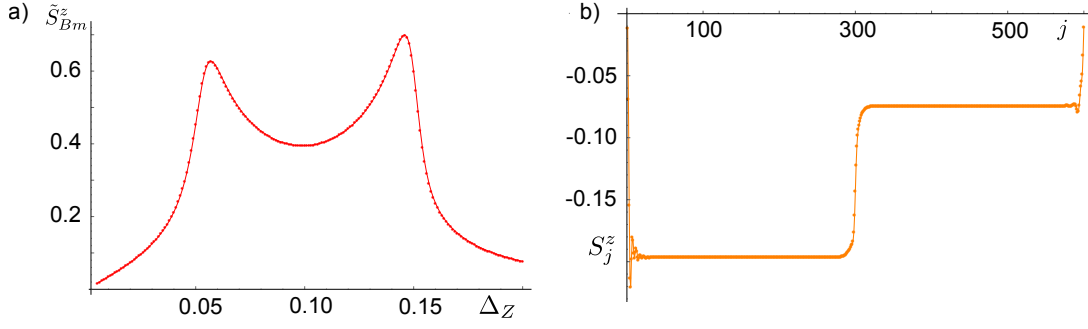
Figure 11. The same as in Fig. 10, however, here, both sections of the NW have the same strength of the SOI ($\alpha = 0.3$) and the same strength of Zeeman energy. However, the proximity-gap is non-uniform: *i.e.* the right (left) section has $\Delta_{SC} = 0.15$ ($\Delta_{SC} = 0.05$). As a result, in panel (a), there are two peaks in $\tilde{S}^z_{Bm}$, which corresponds to two values at which each of sections changes from the trivial to the topological phase. (b) The z-component of the local spin density S^z_j saturates at two different values at the left and right sections, which motivates us to introduce $S^z_{0<}$ and $S^z_{0>}$ for each section separately ($\Delta_Z = 0.10$).

Signatures of topological phase transition in bulk values of spin

So far we have focused on signatures of the topological phase transition to be detected in the boundary spin. However, the bulk values of the spin polarization along the magnetic field, S^z_0, also carries the information about the phase transition in finite-size systems. To focus on bulk properties only and to exclude any influence of boundary effects, we impose now periodic boundary conditions on the system, forming a NW ring. In this case the system is translationally invariant and it does not matter at which point one computes the bulk value of the spin polarization S^z_{PBC}. In finite-size systems, we always observe a sharp discontinuity in S^z_{PBC} at the point of the topological phase transition, $\Delta_Z = \Delta^c_Z$, see Fig. 12. In contrast to the boundary spin, this discontinuity always takes place at Δ^c_Z independent of the system size. However, the value of the jump ΔS^z_{PBC} in S^z_{PBC} depends on the size of the system. We analyzed the value of the jump as a function of system size N and conclude that it can be fitted best by an $1/N$ dependence. We note that the results of this subsection obtained for bulk states with periodic boundary conditions are closely related to the ones obtained for bulk states in Ref. [31]. In particular, the sign reversal of the spin polarization of the bulk state with zero momentum is responsible for the jump in S^z_{PBC}. In stark contrast, the features of the boundary spin $\tilde{S}^z_{Bm}$ are due to boundary effects and thus are of different physical origin.
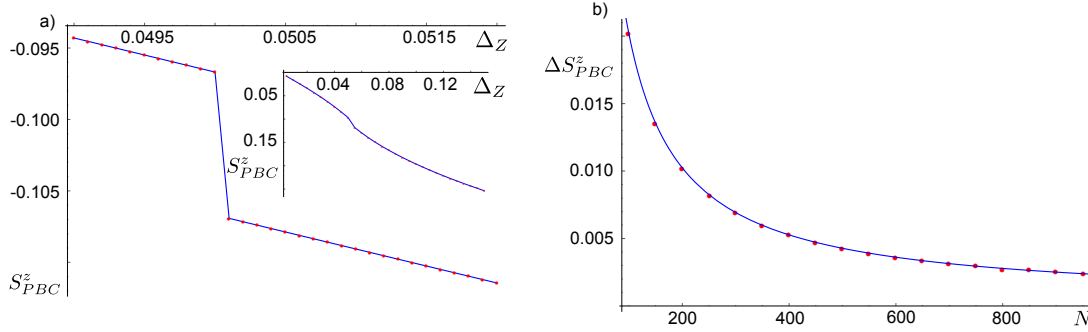

Figure 12. (a) Component of spin polarization along the z axis, S^z_{PBC}, as a function of Zeeman energy in the system with periodic boundary conditions. Away from the topological phase transition point Δ^c_Z, S^z_{PBC} is a linear function of Δ_Z. The discontinuity in spin polarization, ΔS^z_{PBC}, occurs exactly at Δ^c_Z. (b) The size of the jump ΔS^z_{PBC} is inversely proportional to the system size N. Numerical results (red dots) are fitted by the analytical formula $\Delta S^z_{PBC} \propto 1/N$ (blue curve). The system parameters are chosen to be $\alpha = 0.3$, $\Delta_{SC} = 0.05$, $\mu = 0$, and $m = N/2$